Synthetic Metals 160 (2010) 510–515

Contents lists available at ScienceDirect

Synthetic Metals

journal homepage: www.elsevier.com/locate/synmet

Organic field effect transistors based on 5,10,15,20-tetrakis(4-pentyloxyphenyl)porphyrin single crystal

Pan Ma[a], Yanli Chen[c], Xue Cai[a], Hailong Wang[a], Yuexing Zhang[a], Yingning Gao[a], Jianzhuang Jiang[a,b,*]

[a] Department of Chemistry, Shandong University, Jinan 250100, PR China
[b] Department of Chemistry, University of Science and Technology Beijing, Beijing 100083, PR China
[c] Department of Chemistry, University of Jinan, Jinan 250022, PR China

ARTICLE INFO

Article history:
Received 6 November 2009
Accepted 30 November 2009
Available online 6 January 2010

Keywords:
Porphyrin
Single crystal
Organic field effect transistor
Density functional theory

ABSTRACT

Diffusion of methanol into the chloroform solution of metal free 5,10,15,20-tetrakis(4-pentyloxyphenyl)porphyrin H_2TPOPP yields large single crystals with length as long as 1.5 mm, which allow the fabrication of single crystal-based organic field effect transistors (OFETs). These single crystal-based devices were revealed to exhibit relatively good OFET performance with the carrier mobility for hole of 0.0018 $cm^2 V^{-1} s^{-1}$ and current modulation of 10^4. In addition to confirming the tetrappyrole nature, single crystal X-ray diffraction analysis also reveals the planar two-dimensional supramolecular structures formed via porphyrin molecules in the head-to-tail manner through C–H···O interaction between oxygen atom and pyrrole hydrogen atom as well as p(O)–π(phenyl) interaction between the meso-attached phenyloxy groups of neighboring porphyrin molecules in the single crystal. This results in effective intermolecular interaction due to the significant participation of phenyloxy groups to the HOMO of the central porphyrin core as revealed by density functional theory (DFT) analysis and in turn is responsible for the relatively good OFET performance in terms of carrier mobility for hole in the direction parallel to the aromatic porphyrin ring. Density functional theory (DFT) calculation also reproduces the experimentally revealed carrier mobility for hole in the single crystal of H_2TPOPP. The present work, representing our continuous efforts in understanding the relationship between molecular structure, crystal packing, and OFET performance of tetrapyrrole organic semiconductors, will be helpful for attracting further research interest over the semiconducting properties of tetra(aryl)porphyrin compounds for OFET applications.

Crown Copyright © 2009 Published by Elsevier B.V. All rights reserved.

1. Introduction

Organic semiconductors have attracted significant research interest since 1986 when they were first constructed into field effect transistors (OFETs) as active layers [1]. Great industrial interests for these OFETs come from their potential applications in low-cost electronic circuits such as large area and flexible displayer, active-matrix electronic-paper, and smart cards and price tags [2–11]. Despite that the performance of organic semiconductor-based FETs achieved thus far can still not completely compete with the widely utilized inorganic analogues, significant progress has been made in the past two decades in this field. In addition to paying great efforts in continuously searching for novel organic semiconductors with good OFET performance, understanding the relationship between molecular structure, crystal packing, and device performance still remains a great challenge for chemists and material scientists.

Among various organic semiconductors, artificial phthalocyanine derivatives have been the focus of the most intensively studied small molecule organic semiconductor [12–19]. In good contrast, porphyrins as another species of the most important tetrapyrrole derivatives have been relatively less investigated for their semiconducting properties. Despite the investigation over the semiconductor properties of some peripherally substituted porphyrin compounds via indirect pulse-radiolysis time-resolved microwave conductivity technique (PR-TRMC) as early as in 1991 [20], fabrication of OFET devices from porphyrin compounds still remains rare, limited to very few scaffolds such as 2,3,7,8,12,13,17,18-octaethyl-porphyrin and tetrabenzoporphyrin derivatives with planar molecular structure. In 2003, Noh et al. fabricated the epitaxially grown crystalline film of 2,3,7,8,12,13,17,18-octaethyl-porphyrinato platinum PtOEP into OFETs [21]. Later, Minari et al. fabricated a series of 2,3,7,8,12,13,17,18-octaethyl-porphyrinato metal complexes MOEP (M = Co, Cu, Zn, Pd) into single crystal-based

* Corresponding author at: Department of Chemistry, University of Science and Technology Beijing, Beijing 100083, PR China. Tel.: +86 0531 8836 4088; fax: +86 0531 8856 5211.
E-mail addresses: jzjiang@sdu.edu.cn, jianzhuang@ustb.edu.cn (J. Jiang).

0379-6779/$ – see front matter. Crown Copyright © 2009 Published by Elsevier B.V. All rights reserved.
doi:10.1016/j.synthmet.2009.11.040

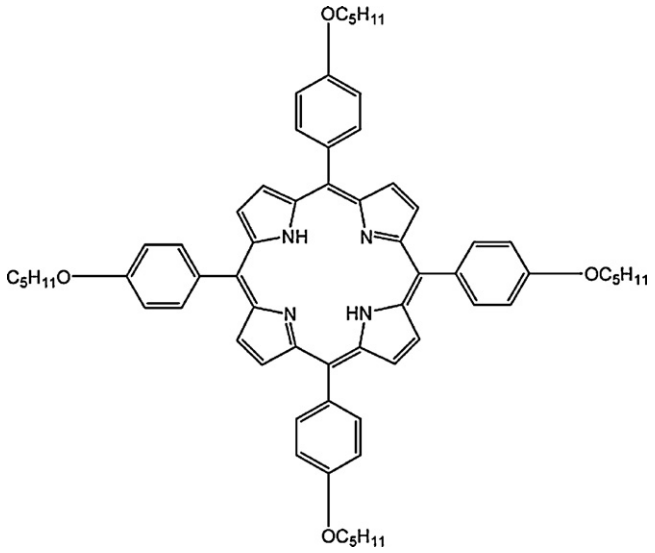

Scheme 1. Schematic molecular structure of metal free tetrakis(4-pentyloxyphenyl)porphyrin H_2TPOPP.

Table 1
Crystallographic data for H_2TPOPP.

	Compound
Formula	$C_{64}H_{70}O_4N_4$
M_r	959.24
Crystal size [mm^3]	0.20 × 0.15 × 0.10
Crystal system	Monoclinic
Space group	$P2_1/c$
a [Å]	14.27(3)
b [Å]	16.52(3)
c [Å]	12.43(2)
α [°]	90.00
β [°]	93.58(3)
γ [°]	90.00
V [Å^3]	2924(9)
Z	2
$F(0\,0\,0)$	1028
ρ_{calcd} [mg m^{-3}]	1.090
μ [mm^{-1}]	0.068
θ range [°]	1.89 to 25.00
Total no. of reflns.	21326
No. of indep. reflns.	4409 (R_{int} = 0.0320)
Parameters	290
$R1$ [$I > 2\sigma(I)$]	0.0706
$wR2$ [$I > 2\sigma(I)$]	0.2059
Goodness of fit	1.077

OFET devices, with the largest carrier mobility of 0.20 cm^2 V^{-1} s^{-1} obtained from CoOEP single crystal [22]. Since 2004, several groups have studied the performance of OFET devices fabricated from tetrabenzoporphyrin derivatives MTBP (M = 2H, Ni, Cu) using a soluble precursor method [23–29]. Until 2008, Che et al. fabricated OFETs from a series of porphyrinato platinum complexes and tried to establish correlation between the peripheral substituents, film structure, and charge mobility [30]. It is worth noting that the carrier mobility for hole recorded for the porphyrin-based OFET devices is about in the range of 10^{-6} to 10^{-1} cm^2 V^{-1} s^{-1}. Surprisingly, the device fabricated from the spin coating film of metal free 5,10,15,20-tetra(phenyl)porphyrin, H_2TPP, was revealed to exhibit carrier mobility for hole as high as 0.007 cm^2 V^{-1} s^{-1} [31]. To the best of our knowledge, this is the sole report on the tetra(aryl)porphyrin-based OFETs. Despite the lack of any information about the molecular structure and packing in their spin coating film, it appears that the four bulky aryl groups attached at the meso positions of porphyrin ring with a large dihedral angle with respect to the central conjugated porphyrin ring in tetra(phenyl)porphyrins does not prevent effective π–π interaction between neighboring H_2TPP molecules according to Checcoli et al.

To get insight into the semiconducting nature of tetra(aryl)porphyrin derivatives, in the present paper, we describe the fabrication of OFETs from single crystals of metal free 5,10,15,20-tetrakis(4-pentyloxyphenyl)porphyrin H_2TPOPP (Scheme 1). These single crystal-based devices were revealed to exhibit relatively high carrier mobility for hole of 1.8×10^{-3} cm^2 V^{-1} s^{-1} in the direction parallel to the aromatic porphyrin ring. Single crystal X-ray diffraction analysis reveals that metal free porphyrin molecules form a two-dimensional planar supramolecular structure in a head-to-tail manner along the *b*-axis direction through C–H···O interaction between oxygen atom and pyrrole hydrogen atom as well as p(O)–π(phenyl) interaction between the meso-attached phenyloxy groups of neighboring porphyrin molecules in the single crystal. This results in effective intermolecular interaction between neighboring porphyrin molecules due to the significant participation of meso-attached phenyloxy substituents to the HOMO of central porphyrin core as verified by the DFT analysis, in the direction parallel to the conjugated porphryin ring, and in turn is responsible for the relatively higher carrier mobility for hole in the single crystal. Density functional theory (DFT) calculation also reproduces the experimentally revealed charge transport property of this compound in terms of carrier mobility for hole in single crystals. The present work, representing our continuous efforts in understanding the relationship between molecular structure, crystal packing, and OFET performance of tetrapyrrole organic semiconductors [16–19,32,33], will be helpful for attracting further research interests over the semiconducting properties of porphyrin derivatives, in particular tetra(aryl)porphyrin compounds for OFET applications.

2. Experimental

2.1. Materials

All reagents and solvents were used as received. The metal free porphyrin H_2TPOPP was prepared according to the published procedure [34]. Single crystals of this compound were obtained by diffusion of methanol into the chloroform solution of H_2TPOPP.

2.2. X-ray crystallographic analyses of H_2TPOPP

Crystal data and details of data collection and structure refinement are given in Table 1. Data were collected on a Bruker SMART CCD diffractometer with an Mo K_α sealed tube (λ = 0.71073 Å) at 293 K, using a ω scan mode with an increment of 0.3°. Preliminary unit cell parameters were obtained from 45 frames. Final unit cell parameters were obtained by global refinements of reflections obtained from integration of all the frame data. The collected frames were integrated using the preliminary cell-orientation matrix. The SMART software was used for collecting frames of data, indexing reflections, and determining lattice constants, SAINT-PLUS was used for integration of intensity of reflections and scaling, SADABS was used for absorption correction [35], and SHELXL was used for space group and structure determination, refinements, graphics, and structure reporting [36]. CCDC-715535 contains the supplementary crystallographic data for this article. These data can be obtained free of charge from the Cambridge Crystallographic Data Centre via http://www.ccdc.cam.ac.uk/data_request/cif.

2.3. Measurements

^{1}H NMR spectra were recorded on a Bruker DPX 300 spectrometer (300 MHz) in $CDCl_3$ using the residual solvent resonance of $CHCl_3$ at 7.26 ppm relative to that of SiMe4 as internal reference. IR spectra were recorded as KBr pellets using a Bio-Rad FTS-165 spectrometer with 2 cm^{-1} resolution. Electronic absorption spectra were recorded on a Hitachi U-4100 spectrophotometer. SEM images were obtained using a HITACHI S-520 scanning electron microscopy. For SEM imaging, Au (1–2 nm) was sputtered onto the substrate to prevent charging effects and to improve the image clarity. Electrochemical measurements were carried out with a BAS CV-50W voltammetric analyser. The cell comprised inlets for a glassy carbon disk working electrode of 3.0 mm in diameter and a silver-wire counter electrode. The reference electrode was Ag/Ag^+ (0.01 mol dm^{-3}), which was connected to the solution by a Luggin capillary whose tip was placed close to the working electrode. It was corrected for junction potentials by being referenced internally to the ferrocenium/ferrocene (Fc^+/Fc) couple [$E_{1/2}$ (Fc^+/Fc) = 0.50 V versus SCE]. Typically, a 0.1 mol dm^{-3} solution of $[Bu_4N][ClO_4]$ in CH_2Cl_2 containing 0.5 mmol dm^{-3} of sample was purged with nitrogen for 10 min, then the voltammograms were recorded at ambient temperature. The scan rate was 20 and 10 mV s^{-1} for CV and DPV, respectively. The electric characteristics of these devices were measured in air. The current–voltage characteristics were obtained with a Hewlett-Packard (HP) 4140B parameter analyser at room temperature. Substrates used in the present study were successively cleaned with pure water, acetone, and ethanol.

3. Results and discussion

3.1. X-ray single crystal structure

Metal free 5,10,15,20-tetrakis(4-pentyloxyphenyl)porphyrin with four 4-pentyloxyphenyl groups at the meso positions of porphyrin ring, H_2TPOPP, was synthesized from the reaction between 4-pentyloxybenzaldehyde and pyrrole in propinonic acid following the published procedure [34]. The newly prepared porphyrin compound was characterized with a wide range of spectroscopic methods including ^{1}H NMR, electronic absorption, and IR spectroscopy (Supporting information). Diffusion of methanol into the chloroform solution of this compound yielded large size lozenge shaped shiny purple crystals with 0.1–1.5 mm in length, 0.1–1.5 mm in width, and 10–30 μm in thickness. The crystal and molecular structure of this metal free porphyrin derivative were determined by single crystal X-ray diffraction analysis. H_2TPOPP crystallizes in the monoclinic system with a $P2_1/c$ space group with two molecules in a unit cell. The crystal data are summarized in Table 1. Fig. S4 (Supporting information) shows the molecular structure of H_2TPOPP, from which its tetrapyrrole nature and molecular dimension are clearly revealed.

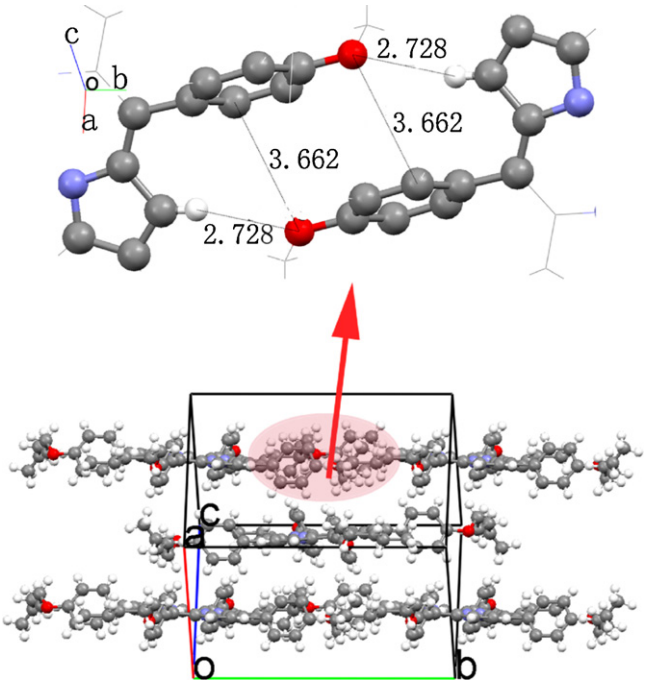

Fig. 1. Crystal packing diagram for H_2TPOPP in the direction parallel to the porphyrin ring.

As revealed in the crystal packing diagram of this metal free porphyrin H_2TPOPP [Figs. 1 and S5 (Supporting information)], metal free porphyrin molecules first form a two-dimensional planar supramolecular structure parallel to porphyrin ring in a head-to-tail manner along the *b*-axis direction through C–H···O interaction between oxygen atom and pyrrole hydrogen atom as well as p(O)–π(phenyl) interaction between the meso-attached phenyloxy groups of neighboring porphyrin molecules in the single crystal, leading to a very short separation between the neighboring metal free porphyrin molecules with the phenyloxy–phenyloxy distance of 3.368 Å. Nevertheless, in the direction perpendicular to the porphyrin ring, these two-dimensional planar supramolecular structures further stack into a three-dimensional face-to-face stacking supramolecular structure depending on weak C–H···π interaction. In this three-dimensional supramolecular structure, the separation between the two C_2 axes of the two closest H_2TPOPP units in two neighboring planar two-dimensional supramolecular structures is 8.931/9.438 Å, indicating the lack of any π–π overlapping between these porphyrin rings in the neighboring two-dimensional planar supramolecular structures on the basis of

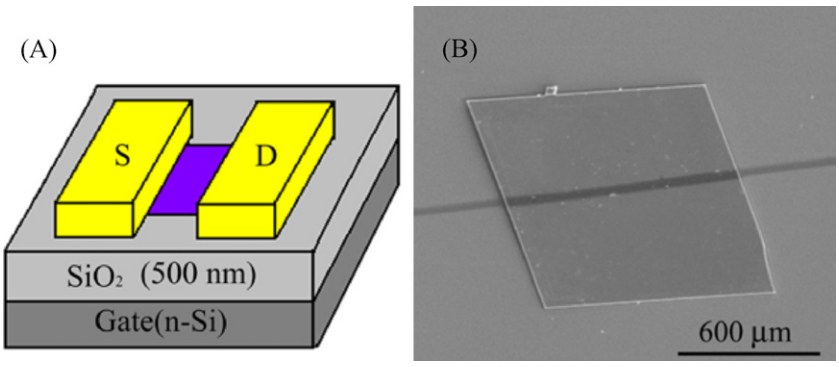

Fig. 2. (A) Schematic diagram for the porphyrin single crystal-based OFET device and (B) the SEM image of a device.

Table 2
Half-wave redox potentials of H_2TPOPP in CH_2Cl_2 containing 0.1 M TBAP.

Compound	Oxd_2	Oxd_1	Red_1	Red_2 [a]	$\Delta E^\circ_{1/2}$ [b]
H_2TPOPP	1.06	0.85	−1.21	−1.59	2.06

[a] Recorded by DPV.
[b] $\Delta E^\circ_{1/2}$ is the potential difference between the first oxidation and first reduction processes, i.e. the HOMO–LUMO gap of corresponding molecule.

molecular dimension. As a consequence, growing in this direction for single crystals during the crystallization process is also limited. As confirmed by the single crystal X-ray analysis result, the longitudinal direction of the crystals for H_2TPOPP is actually in a parallel manner with the conjugated porphyrin ring (Fig. 1). On the basis of fabrication of single crystal-based OFET device as detailed in Fig. 2, the electrical conduction was actually measured in the direction parallel instead of perpendicular to the conjugated porphyrin ring.

3.2. Electrochemical properties

The electrochemical behavior of H_2TPOPP was investigated by cyclic voltammetry (CV) and differential pulse voltammetry (DPV) in CH_2Cl_2. This compound displays two one-electron oxidations labeled as Oxd_1 and Oxd_2 and two one-electron reductions labeled as Red_1 and Red_2 within the electrochemical window of CH_2Cl_2. The separation between the reduction and oxidation peak potentials for each process is 65–90 mV. The half-wave redox potential values vs. SCE are summarized in Table 2. On the basis of the electrochemical result, the HOMO and LUMO energy for this metal free porphyrin compound are −5.77 and −3.71 eV, respectively. As can be seen, the HOMO of H_2TPOPP well matches the Fermi energy level of gold (−5.1 eV), indicating the relatively easy hole injection from the Au source electrode to the crystal of H_2TPOPP [37].

3.3. OFET properties

The OFET devices based on individual single crystal of H_2TPOPP with millimeter size were fabricated on bare Si/SiO_2 substrates with top contact configuration (Fig. 2) [38]. The heavily doped silicon layer functioning as the gate electrode and Au thin films as the source/drain electrodes were thermally evaporated onto the H_2TPOPP single crystal by use of a shadow mask. The electrodes have width (W) of 1.28 mm (depending on the size of the single crystal) and channel length (L) of 55 μm. The SiO_2 dielectric layer of 500 nm is of a capacitance per unit area of 10 nF cm^{-2}. All the properties of the transistors were measured with a source/drain current along the longest dimension of the crystal which is actually parallel to the conjugated porphyrin ring according to the X-ray diffraction analysis. The devices were dried in vacuum at room temperature for 24 h before electronic testing, which was carried out at ambient temperature and open to air.

The OFET devices show typical p-channel characteristic as shown in Fig. 3. It is worth noting that even using Au as the source/drain electrodes, a relatively large electron injection barrier and therefore some contact resistance still existed as videnced by slight curvatures seen at low V_{ds} in the output plot of the OFET device [39]. The carrier mobility (μ) was calculated by using the saturation region transistor equation, $I_{ds} = (W/2L)\mu C_0 (V_g - V_t)^2$, where I_{ds} is the source–drain current, V_g the gate voltage, C_0 the capacitance per unit area of the dielectric layer, and V_t the threshold voltage [40]. Experimental results indicate that on the bare SiO_2/Si substrate, the devices fabricated from H_2TPOPP single crystal display relatively good OFET performance with the carrier mobility for hole of 1.8×10^{-3} cm^2 V^{-1} s^{-1}, current modulation of 10^4, and threshold voltage of −14.5 V.

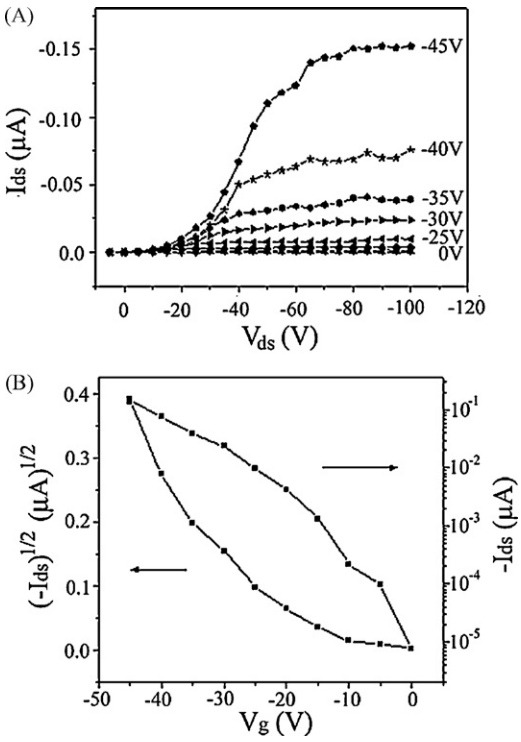

Fig. 3. Drain–source current (I_{ds}) versus drain–source voltage (V_{ds}) characteristic at different gate voltage (A) and transfer characteristic at $V_{ds} = -100$ V and (B) for the OFET of H_2TPOPP on the bare SiO_2/Si substrate.

3.4. DFT calculations

To understand the charge transport property of H_2TPOPP in single crystal, DFT calculation on the electronic coupling between the HOMO orbitals of dimeric molecules connected in a head-to-tail manner in the two-dimensional planar supramolecular structure in single crystal of H_2TPOPP was carried out (Fig. 4). As can be seen, in addition to distributing over the central conjugated macrocycle ring, the HOMO of H_2TPOPP also distributes on the phenyl group and oxygen atom of the 4-pentyloxyphenyl substitutents, leading to an effective coupling over the HOMO orbitals between neighbouring H_2TPOPP molecules through phenyl group and oxygen atom of the 4-pentyloxyphenyl substitutents along the b-axis direction in the planar two-dimensional supramolecular structures in the single crystal. As clearly shown in Fig. 4, the orbital nodes distributed on the oxygen atom and the carbon atom of phenyl group connected with the oxygen atom in one H_2TPOPP molecule display bonding interaction with the orbital nodes of corresponding atoms of the neighbouring H_2TPOPP molecule due to their close distance and more importantly the appropriate orientation of the 4-pentyloxyphenyl groups. In addition, the orbital nodes distributed on the two oxygen atoms of H_2TPOPP dimer in the direction perpendicular to b-axis in the planar two-dimensional plane is also of some electron coupling, which however is much weaker in comparison with that in the b-axis direction due to their much larger separation and inappropriate orientation. In good contrast, there is almost no electronic coupling between porphyrin molecules in different planar two-dimensional supramolecular structures due to the relatively large plane-to-plane separation and in particular completely slipping between porphyrin molecules of different plane [Figs. 4 and S5 (Supporting information)]. As a consequence, the favorable transfer route for hole in the single crystal of H_2TPOPP is along the b-axis direction in the planar two-dimensional supramolecular structure depending on the effective intermolecular interaction in the head-to-tail manner instead of π–π stacking manner in the

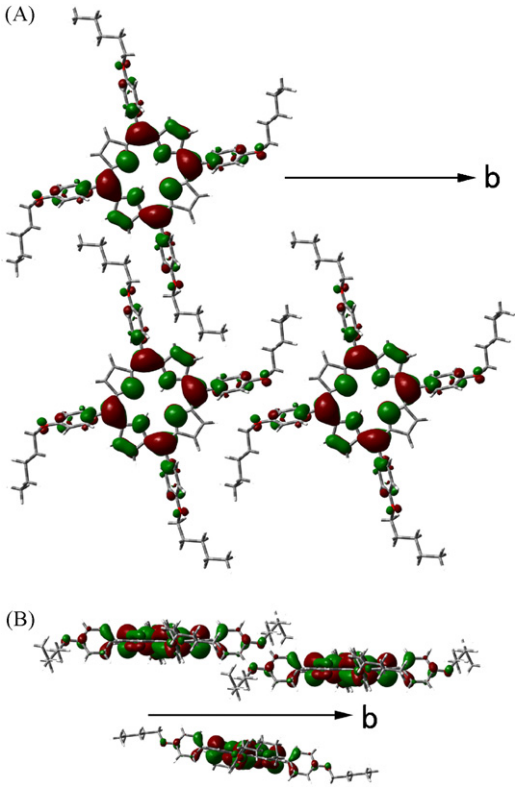

Fig. 4. Schematic diagram of the electronic coupling for the HOMO of H_2TPOPP molecules in the single crystal in the planar two-dimensional supramolecular structure (A) and between neighboring planar two-dimensional supramolecular structure (B).

single crystal.

To have a quantitative insight into the charge mobility for hole of H_2TPOPP single crystal, the electronic couplings (V) and the charge transfer mobility for hole of H_2TPOPP is also calculated on the basis of its single crystal structure using an incoherent hopping model [41]. According to the calculation result, the vertical ionization energy (IE_v) and vertical electronic affinity (EA_v) for H_2TPOPP are 5.706 and 0.978 eV, respectively. It is well known that molecular compounds with large vertical electron affinity EA_v will show advantage as *n*-type organic semiconductor in terms of charge injection while those with small IE_v favor *p*-type semiconductor [42,43]. In particular, according to Newman et al. [44], molecular materials with the electronic affinity locating in the range of 3.0–4.0 eV, which is close to the work function of gold electrode (around 5.1 eV), can ensure efficient electron injection from gold electrode and therefore act as good *n*-type semiconductor for OFETs. In the present case, the vertical ionization energy of H_2TPOPP is obviously much closer to the work function of gold electrode (around 5.1 eV) than its vertical electronic affinity, indicating the easier hole injection but harder electron injection from the gold source electrode into semiconductor layer composed of H_2TPOPP when being fabricated into OFETs. This in turn suggests the better *p*-type semiconducting property over *n*-type of this compound. This corresponds well with the experimental findings that the H_2TPOPP single crystal-based OFET devices display relatively higher carrier mobility for hole as described above. The calculated reorganization energy for hole (λ_+) transfer processes of H_2TPOPP is 0.234 eV. With its X-ray single crystal structure, the charge transfer integrals between one randomly selected molecule and all its possible neighbors are calculated in Table S1 (Supporting information). According to the calculation result, among all the possible routes the largest transfer integral for hole in H_2TPOPP single crystal occurs in the two neighbouring molecules along *b*-axis, amounting to 2.531 meV [Fig. S6 (Supporting information)]. The intrinsic mobility for hole (μ_+) is therefore 2.7×10^{-3} cm^2 V^{-1} s^{-1}. This calculation result is also in good accordance with the experimentally revealed one, 1.8×10^{-3} cm^2 V^{-1} s^{-1}.

4. Conclusions

In summary, novel organic field effect transistors were fabricated from H_2TPOPP single crystals, which exhibit relatively high carrier mobility, in the direction parallel to the aromatic porphyrin ring, and current modulation value. In particular, single crystal X-ray diffraction analysis reveals the close intermolecular interaction in the direction parallel to the conjugated porphryin ring through C–H···O interaction between oxygen atom and pyrrole hydrogen atom as well as p(O)–π(phenyl) interaction between the meso-attached phenyloxy groups of neighboring porphyrin molecules in the single crystal, which in turn results in the effective charge transport along the *b*-axis direction. The present work, representing our continuous efforts in understanding the relationship between molecular structure, crystal packing, and OFET performance of tetrapyrrole organic semiconductors, will be helpful for attracting further research interest over the semiconducting properties of porphyrin derivatives, in particular tetra(aryl)porphyrin compounds for OFET applications.

Acknowledgments

Financial support from the Natural Science Foundation of China (Grant No. 20325105, 20431010, 20501011), Ministry of Education of China, and Shandong University is gratefully acknowledged. We are also grateful to the Shandong Province High Performance Computing Centre for a grant of computer time.

Appendix A. Supplementary data

Supplementary data associated with this article can be found, in the online version, at doi:10.1016/j.synthmet.2009.11.040.

References

[1] A. Tsumura, H. Koezuka, T. Ando, Appl. Phys. Lett. 49 (1986) 1210–1212.
[2] G. Horowitz, Adv. Mater. 10 (1998) 365–377.
[3] D. Fichou, J. Mater. Chem. 10 (2000) 571–588.
[4] H.E. Katz, Z. Bao, J. Phys. Chem. B 104 (2000) 671–678.
[5] H.E. Katz, Z. Bao, S.L. Gilat, Acc. Chem. Res. 34 (2001) 359–369.
[6] F. Würthner, Angew. Chem. Int. Ed. 40 (2001) 1037–1039.
[7] C.D. Dimitrakopoulos, P.R.L. Malenfant, Adv. Mater. 14 (2002) 99–117.
[8] J. Veres, S. Ogier, G. Lloyd, D. de Leeuw, Chem. Mater. 16 (2004) 4543–4555.
[9] Y. Sun, Y. Liu, D. Zhu, J. Mater. Chem. 15 (2005) 53–65.
[10] H. Sirringhaus, Adv. Mater. 17 (2005) 2411–2425.
[11] Z. Bao, Adv. Mater. 12 (2000) 227–230.
[12] K. Xiao, Y.Q. Liu, X.B. Huang, Y. Xu, G. Yu, D.B. Zhu, J. Phys. Chem. B 107 (2003) 9226–9230.
[13] J. Zhang, J. Wang, H. Wang, D. Yan, Appl. Phys. Lett. 84 (2004) 142–144.
[14] Z. Bao, A.J. Lovinger, A. Dodabalapur, Appl. Phys. Lett. 69 (1996) 3066.
[15] Z. Bao, A.J. Lovinger, J. Brown, J. Am. Chem. Soc. 120 (1998) 207–208.
[16] W. Su, J. Jiang, K. Xiao, Y. Chen, Q. Zhao, G. Yu, Y. Liu, Langmuir 21 (2005) 6527–6531.
[17] Y. Chen, W. Su, M. Bai, J. Jiang, J. Am. Chem. Soc. 127 (2005) 15700–15701.
[18] R. Li, P. Ma, S. Dong, X. Zhang, Y. Chen, X. Li, J. Jiang, Inorg. Chem. 46 (2007) 11397–11404.
[19] Y. Gao, P. Ma, Y. Chen, Y. Zhang, Y. Bian, X. Li, J. Jiang, C. Ma, Inorg. Chem. 48 (2009) 45–54.
[20] P.G. Schouten, J.M. Warman, M.P. de Haas, M.A. Fox, H.L. Pan, Nature 353 (1991) 736–737.
[21] Y.Y. Noh, J.J. Kim, Y. Yoshida, K. Yase, Adv. Mater. 15 (2003) 699–702.
[22] T. Minari, M. Seto, T. Nemoto, S. Isoda, K. Tsukagoshi, Y. Aoyagi, Appl. Phys. Lett. 91 (2007) 123501.
[23] S. Aramaki, Y. Sakai, N. Ono, Appl. Phys. Lett. 84 (2004) 2085–2087.
[24] P.B. Shea, J. Kanicki, N. Ono, J. Appl. Phys. 98 (2005) 014503.
[25] P. Shea, A.R. Johnson, N. Ono, J. Kanicki, IEEE Trans. Electron. Dev. 52 (2005) 1497–1503.

[26] P.B. Shea, C. Chen, J. Kanicki, L.R. Pattison, P. Petroff, H. Yamada, N. Ono, Appl. Phys. Lett. 90 (2007) 233107.
[27] P.B. Shea, J. Kanicki, L.R. Pattison, P. Petroff, M. Kawano, H. Yamada, N. Ono, J. Appl. Phys. 100 (2006) 034502.
[28] P.B. Shea, L.R. Pattison, M. Kawano, C. Chen, J. Chen, P. Petroff, D.C. Martin, H. Yamada, N. Ono, J. Kanicki, Synth. Met. 157 (2007) 190–197.
[29] A.S. Dhoot, S. Aramaki, D. Moses, A. Heeger, Adv. Mater. 19 (2007) 2914–2917.
[30] C. Che, H. Xiang, S.S. Chui, Z.X. Xu, V.A.L. Roy, J.J. Yan, W.F. Fu, P.T. Lai, I.D. Willianms, Chem. Asian J. 3 (2008) 1092–1103.
[31] P. Checcoli, G. Conte, S. Salvatori, R. Paolesse, A. Bolognesi, A. Berliocchi, F. Brunetti, A. D'Amico, A. Di Carlo, P. Lugli, Synth. Met. 138 (2003) 261–266.
[32] X. Cai, Y. Zhang, D. Qi, J. Jiang, J. Phys. Chem. A 113 (2009) 2500–2506.
[33] Y. Zhang, X. Cai, Y. Bian, X. Li, J. Jiang, J. Phys. Chem. C 112 (2008) 5148–5159.
[34] J. Ning, H. Zhao, N. Zhou, Youji Huaxue 25 (2005) 1381–1385.
[35] G.M. Sheldrick, SADABS, A Software for Empirical Absorption Correction, University of Göttingen, Germany, 1997.
[36] SHELXL Reference Manual, Version 5.1, Bruker Analytical X-Ray Systems, Madison, WI, 1997.
[37] J. Zaumseil, H. Sirringhaus, Chem. Rev. 107 (2007) 1296–1323.
[38] Q.X. Tang, H.X. Li, M. He, W.P. Hu, C.M. Liu, K.Q. Chen, C. Wang, Y.Q. Liu, D.B. Zhu, Adv. Mater. 18 (2006) 65–68.
[39] H.F. Wang, Y.G. Wen, X.D. Yang, Y. Wang, W.Y. Zhou, S.M. Zhang, X.W. Zhan, Y. Liu, Z.G. Shuai, D.B. Zhu, ACS Appl. Mater. Interfaces 1 (2009) 1122–1129.
[40] M.J. Cook, I. Chambrier, Porphyrin Handbook, in: K.M. Kadsh, K.M. Smith, R. Guilard (Eds.), Phthalocyanines: Properties and Materials, vol. 17, Elsevier Science, USA, 2003, pp. 37-127.
[41] W. Paulus, H. Schober, S. Eibl, M. Johnson, T. Berthier, O. Hernandez, M. Ceretti, M. Plazanet, K. Conder, C. Lamberti, J. Am. Chem. Soc. 130 (2008) 16080–16085.
[42] Y. Zhang, X. Cai, J. Jiang, J. Phys. Chem. C 112 (2008) 14579–14588.
[43] M.-Y. Kuo, H.-Y. Chen, I. Chao, Chem. Eur. J. 13 (2007) 4750–4758.
[44] C.R. Newman, C.D. Frisbie, D.A. da Silva, J.-L. Bredas, P.C. Ewbank, K.R. Mann, Chem. Mater. 16 (2004) 4436–4451.